EMILIN-1 deficiency promotes chronic inflammatory disease through TGFβ signaling alteration and impairment of the gC1q/α4β1 integrin interaction

Eliana Pivetta [a], Alessandra Capuano [a], Maddalena Vescovo [a], Eugenio Scanziani [b,c], Andrea Cappelleri [b,c], Gian Luca Rampioni Vinciguerra [a,d], Andrea Vecchione [e], Roberto Doliana [a], Maurizio Mongiat [a,1] and Paola Spessotto [a,1]

***a* - Unit of Molecular Oncology,** *Centro di Riferimento Oncologico di Aviano (CRO), IRCCS, Aviano, Italy*
***b* - Department of Veterinary Medicine and Animal Science,** *University of Milan, Milan, Italy*
***c* - Mouse and Animal Pathology Lab (MAPLab),** *Fondazione UniMi, Milan, Italy*
***d* - Department of Cancer Biology and Genetics,** *The Ohio State University, Columbus, OH, USA*
***e* - Faculty of Medicine and Psychology,** *Department of Clinical and Molecular Medicine, University of Rome "Sapienza", Sant'Andrea Hospital, Rome, Italy*

Corresponding to Eliana Pivetta: *Unit of Molecular Oncology, Centro di Riferimento Oncologico di Aviano (CRO), IRCCS, Aviano, Italy.* *epivetta@cro.it.*
https://doi.org/10.1016/j.matbio.2022.06.005

Abstract

Alterations in extracellular matrix (ECM) components that modulate inflammatory cell behavior have been shown to serve as early starters for multifactorial diseases such as fibrosis and cancer. Here, we demonstrated that loss of the ECM glycoprotein EMILIN-1 alters the inflammatory context in skin during IMQ-induced psoriasis, a disease characterized by a prominent inflammatory infiltrate and alteration of vessels that appear dilated and tortuous. Abrogation of EMILIN-1 expression or expression of the EMILIN-1 mutant E933A impairs macrophage polarization and leads to imbalanced tissue homeostasis. We found that EMILIN-1 deficiency is associated with dilated lymphatic vessels, increased macrophage recruitment and psoriasis severity. Importantly, the null or mutant EMILIN-1 background was characterized by the induction of a myofibroblast phenotype, which in turn drove macrophages towards the M1 phenotype. By using the transgenic mouse model carrying the E933A mutation in the gC1q domain of EMILIN-1, which abolishes the interaction with α4- and α9-integrins, we demonstrated that the observed changes in TGFβ signaling were due to both the EMI and gC1q domains of EMILIN-1. gC1q may exert multiple functions in psoriasis, in the context of a final, more consistent inflammatory condition by controlling skin homeostasis via interaction with both keratinocytes and fibroblasts, influencing non-canonical TGFβ signaling, and likely acting on lymphatic vessel structure and function. The analyses of human psoriatic lesions, in which lower levels of EMILIN-1 were present with a very rare association with lymphatic vessels, support the multifaceted role of this ECM component in the skin inflammatory scenario.

Introduction

The extracellular matrix (ECM) is a highly specialized network that provides both mechanical and molecular signals to the cells, functioning as a scaffold for physical structure to the tissues as well as regulating cell proliferation, survival, migration, and differentiation. Due to active communication with cells through the binding to cell surface receptors, the ECM alterations occurring during remodeling in normal tissue repair, as well as in the progression of various diseases, can promote pathological cell behavior [1,2]. Several studies suggest that dysregulated production of ECM modulators plays a key role in

inflammation, supporting the hypothesis that aberrant ECM deposition may condition multifactorial inflammatory diseases including fibrosis and cancer [3,4]. There are examples in which the disruption of the ECM structure and function leads to alterations in cell-matrix interactions that contribute to hyperproliferation of keratinocytes and enhancement of immunoinflammatory responses, ultimately leading to alteration of epidermal homeostasis [5]. In turn, the accumulation of inflammatory cytokines and the release of proteases can alter ECM proteins [6].

Psoriasis is a chronic inflammatory skin disease characterized by the formation of scaly erythematosquamous plaques, epidermal thickening of the viable layers and parakeratotic hyperkeratosis due to dysregulation of keratinocyte proliferation and differentiation [7,8]. Several studies documented that the clinical abnormalities are preceded in the dermis by blood vessel changes with conspicuous dilated hyperpermeable and twisted vessels [9]. In contrast, less is known about the involvement of lymphatic vessels (LVs) in the development of this disease, with lymphangiogenesis apparently following altered angiogenesis [10]. Moreover, inflammation is accompanied by striking changes in the lymphatic vasculature [11], although the molecular mechanisms involved in the regulation of this process are not fully understood. It is known that proinflammatory cytokines, e.g. IL-1 and TNFα induce the expression of the lymphatic growth factors VEGFC and VEGFD in infiltrating cells, thereby supporting inflammatory lymphangiogenesis [11]. The new abnormal LVs exhibit increased leakage and reduced functionality, and most likely promote the persistence of inflammatory cells in the tissue [12,13]. The fact that activation of lymphatic vasculature and the consequent improvement in their clearance function have been associated with a reduction in disease severity points to a crucial role of lymphatic functionality in the resolution of psoriasis [12,14,15].

The elastin microfibrillar interface protein (EMILIN-1), a member of the EMILIN/Multimerin family, is highly expressed in tissues where resilience and elastic recoil are prominent, including the cardiovascular system, lung, kidney, and cornea [16–19]. We have previously shown that dermal fibroblasts express high levels of EMILIN-1 which is then organized in a network, with a characteristic basket-shaped structure around the hair bulb [20]. EMILIN-1 is characterized by the presence of a region homologous to the globular homotrimeric C-terminal domain C1q (gC1q domain) [16,17] which is involved in EMILIN-1 oligomerization [21], and in cell adhesion and migration via interaction with the α4β1 [22] and the closely related α9β1 integrin [20,23]. In addition, the hallmark of the EMILIN family is the presence of the EMI domain at the N terminus [24], which interacts with pro-TGFβ regulating the maturation in its active form [18]. Through integrin interaction, EMILIN-1 provides an ECM cue for proper homeostatic proliferation, particularly in the skin [20]. Accordingly, targeted inactivation of the *Emilin1* gene induces dermal and epidermal hyperproliferation [20], accelerates tumor development and increases the number and size of skin tumors [25], demonstrating the oncosuppressive activity of EMILIN-1 in the preclinically context of skin cancer. Another important direct role is played by EMILIN-1 in the growth and maintenance of LVs [23,26,27]. By exploiting a transgenic mouse model carrying the E933A mutation in the gC1q domain of EMILIN-1, which abolishes the interaction with α4/α9 integrins, we provided evidence for a novel "regulatory structural" role of EMILIN-1 in lymphangiogenesis [28,29]. The integrity of EMILIN-1 was shown to be important also in this context: using an animal model of post-surgical tail lymphedema we demonstrated that the acute phase of acquired lymphedema was correlated to EMILIN-1 degradation due to elastase released by infiltrating neutrophils [27].

In the present study, we took advantage of the mouse model of psoriasis characterized by a conspicuous inflammatory infiltrate [7,8] to investigate the extent to which loss of EMILIN-1 may be a determining factor in the maintenance or exacerbation of an inflammatory process. We demonstrated that the absence of EMILIN-1 leads to a fibrotic state with an increase of the macrophage population, a switch toward a pro-inflammatory M1 phenotype, thus giving rise to a microenvironment consistent with disease development.

Results

EMILIN-1 is impaired in human psoriatic lesions

Excessive proliferation of keratinocytes and infiltration of inflammatory cells, well known and established histopathologic markers of psoriasis, were noted in all human psoriatic lesions analyzed in this study (Fig. 1a, b). Assignment of an arbitrary inflammatory score confirmed that a large amount of neutrophils, lymphocytes and monocytes/macrophages was always present in all patients examined (Fig. 1b). We next assessed the expression of EMILIN-1 in this context. In healthy human skin, the EMILIN-1 fibrils extended from the dermis toward the keratinocytes of the basal layer (Fig. 1c, white arrowheads) and were organized as a network throughout the tissue. In contrast, in the psoriatic dermis the EMILIN-1 fibrils were less prominent or completely absent, and the projections toward the basal keratinocytes completely missing (Fig. 1c). In addition, in healthy human skin EMILIN-1 was closely associated with podoplanin-positive LVs (Fig. 1d). In

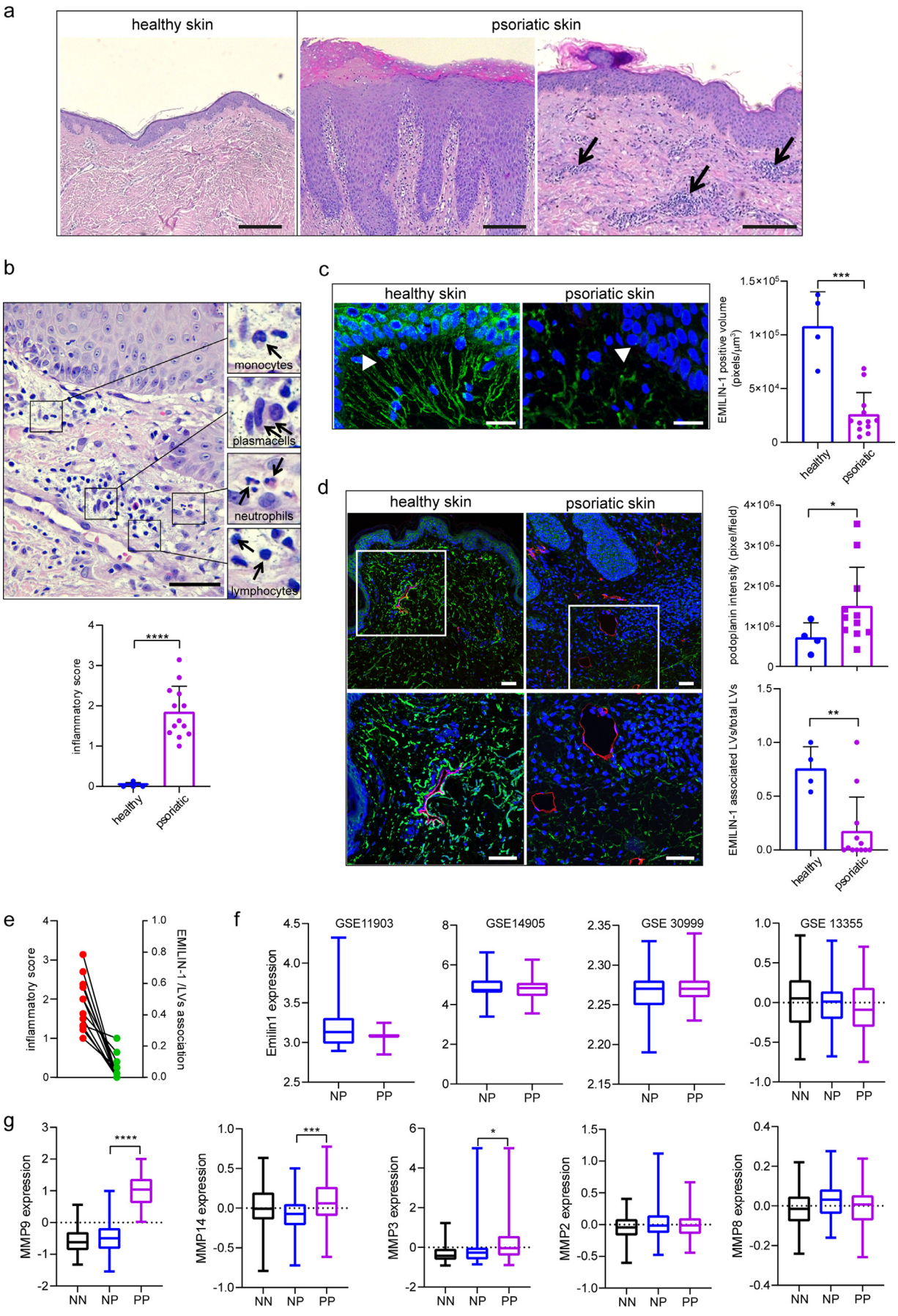

Fig. 1. EMILIN-1 is dysregulated and not associated to LVs in human psoriatic skin. (a) Representative H&E images of FFPE sections of healthy skin (left) and cutaneous psoriatic lesions (middle and right). Arrows indicate the presence of

contrast, a significant reduced amount of EMILIN-1 in proximity of LVs was detected in psoriatic skin (Fig. 1d). Importantly, the association of EMILIN-1 with podoplanin-positive LVs inversely correlated with the extent of inflammatory infiltrate (Fig. 1e). Analyses of microarray dataset deposited by the Collaborative Association Study of Psoriasis (CSAP) [30] indicated that the expression of the EMILIN-1 mRNA was unchanged in normal versus non-lesional and lesional psoriatic skin (Fig. 1f), suggesting that the decreased expression of the protein (Fig. 1c) was due to protein degradation rather than impaired synthesis. Inflammatory cells can secrete proteases capable of degrading ECM components including EMILIN-1 [27,31]. This was in line with the finding that the expression of MMP9, MMP14 and MMP3, known to degrade EMILIN-1 [32], was significantly higher in psoriatic lesion compared to matched non-lesional skin (Fig. 1g). In contrast, the expression of MMP2 and MMP8, which are not involved in EMILIN-1 degradation [32], was unchanged (Fig. 1g).

EMILIN-1 deficiency associates with increased disease severity in an IMQ-induced psoriasis mouse model

To further explore if EMILIN-1 could play a significant role in inflamed skin, wild type ($E1^{+/+}$) and *Emilin1*$^{-/-}$ ($E1^{-/-}$) C57BL/6 mice were shaved and treated with daily applications of imiquimod (IMQ) for four consecutive days to induce psoriasis (Fig. 2a). On day 5, mice were sacrificed and skin tissue was harvested. All treated animals showed the classic signs of psoriasis such as erythema, scaling and thickening (Fig. 2b). Our previous analyses performed on the CD1 strain indicated that the untreated epidermis is per se significantly thicker in $E1^{-/-}$ mice compared to that of $E1^{+/+}$ animals, since EMILIN-1 deficiency causes a hyperproliferative phenotype of keratinocytes [20]. Here, the histological analyses showed increased epidermal thickness in IMQ-treated animals compared to control animals for both genotypes (Fig. 2c, d). Moreover, in untreated $E1^{-/-}$ mice, we occasionally detected moderate focal epidermal hyperplasia characterized by acanthosis and hypergranulosis, resulting in the disappearance of the basement membrane (Fig. 2e). In addition, the absence of EMILIN-1 also associated with a moderate focal hyperproliferation of fibroblasts, which was also present in the upper dermis (Fig. 2e and Supplemental Fig. 1). In analogy with CD1 mice [20], the untreated dermis of all animals was significantly thicker in $E1^{-/-}$ compared to $E1^{+/+}$ mice (Fig. 2c, d).

The histological score evaluating psoriasis-like dermatitis in mice showed that IMQ treatment elicited a stronger effect in $E1^{-/-}$ than in $E1^{+/+}$ mice, especially regarding the presence of pustules or Munro's microabscesses and the parakeratosis of the stratum corneum (Fig. 2e). Of note, parakeratosis, that is a hallmark of human psoriasis, was more and particularly evident in $E1^{-/-}$ mice.

To investigate the possibility that the ECM components were differently altered in the two genotypes because of the induction of psoriasis, we stained the untreated and IMQ-treated skins for two ECM molecules mainly located in the basement membrane (collagen IV and laminin 5) and for the EDA isoform of fibronectin, which is upregulated in the dermis during inflammation. As shown in Supplemental Fig. 2, IMQ treatment did not induce any measurable changes in deposition and pattern of laminin 5 and collagen IV. Expression of EDA was increased after

inflammatory infiltrates in psoriatic skin. (b) Typical appearance of inflammatory infiltrate in a psoriatic lesion. Magnified images of the boxed areas are reported on the right as examples for the peculiar presence of neutrophils, monocytes, lymphocytes, and plasma cells (black arrows). Inflammatory score reported in the graph is calculated as follows: 0=no infiltrate, 1=rare immune cells; 2=poor infiltrate; 3=modest infiltrate; 4=abundant infiltrate. For each sample at least three fields were analyzed and the final score average was reported in the graph. (c) Representative images of EMILIN-1 staining (green) at the interface between dermis and epidermis (nuclei pseudocolored in blue). In healthy skin (left) evident EMILIN-1 fibrils project towards basal layer of keratinocytes (white arrowhead). In cutaneous psoriatic lesions (right) these projections are mostly lacking and the EMILIN-1 staining is reduced. The associated graph represents the quantification of EMILIN-1 positive volume in the whole section field examined (x20). At least four fields per sample were analyzed and the mean value was reported. (d) Immunofluorescence staining for EMILIN-1 (green) and podoplanin (red) in healthy and psoriatic skin (nuclei pseudocolored in blue). A magnification of the boxed areas is shown in the lower panel. A graphical quantification of podoplanin intensity and of EMILIN-1 association with LVs is provided on the right. This association was calculated as the ratio between double positive vessels for EMILIN-1 and podoplanin out of total podoplanin positive vessels. The results reported in the graphs (b, c and d) represent the mean ± SD of 4 healthy subjects and 13 patients affected by psoriasis. Scale bars: 20 μm (c), 50 μm (b and d), 200 μm (a). (e) The graph represents the inverse correlation between patient inflammatory score and EMILIN-1 association with LVs. (f) *EMILIN1* gene expression analyses using the Gene Expression Omnibus (GEO) dataset GSE11903, GSE14905, GSE30999, and GSE13355 in tissues from psoriatic patients with (PP) and without (NP) lesions (n = 58). The analysis of skin in healthy subjects (NN, n = 64) available for GSE13355 was also reported. (g) Gene expression data in the GEO dataset GSE13355 were analyzed for the expression of MMP9, MMP14, MMP3, MMP2 and MMP8. P values were calculated using two-tailed Student's t-test. $^{*}P < 0.05$, $^{**}P < 0.01$, $^{***}P < 0.001$, $^{****}P < 0.0001$. (For interpretation of the references to color in this figure legend, the reader is referred to the web version of this article.)

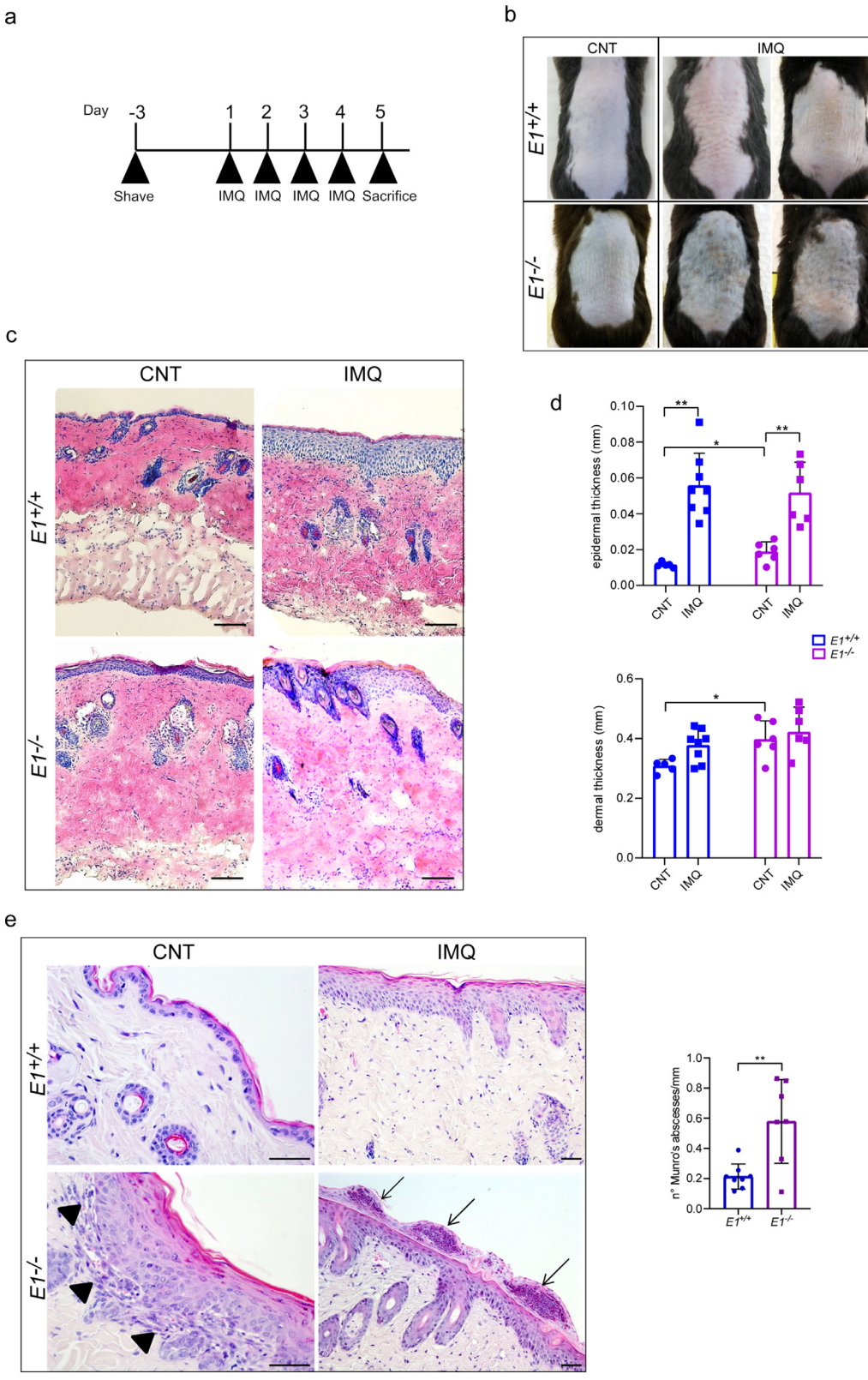

Fig. 2. ***E1*** $^{-/-}$ mice exhibit alterations in skin homeostasis and develop a more severe histologic score after IMQ treatment. (a) Schematic representation of the protocol applied in the IMQ-induced psoriasis mouse model. (b) Macroscopic view of mouse skin at the end of IMQ treatment. Representative images are shown. (c) H&E staining of cryostat sections of untreated (CNT) and IMQ-treated (IMQ) mouse skin. (d) Analysis of epidermal and dermal thickness in untreated and

treatment but without any obvious difference between the two genotypes.

Given the role of EMILIN-1 in lymphangiogenesis [23,26,29] and its reduction in psoriasis (Fig. 1), we next examined the lymphatic microvasculature. The number of Lyve1 positive vessels was higher in IMQ-treated animals compared to control animals in both genotypes (Fig. 3). Nevertheless, we observed a slightly increased density and statistically higher volume of Lyve1 positive vessels in untreated $E1^{-/-}$ mice, indicating the presence of already enlarged LVs even in the absence of a psoriasis stimulus (Fig. 3). These changes were also evident in both treated and untreated $E1^{-/-}$ mice when VEGFR3 was used as an additional marker of LVs (Supplemental Fig. 3). In general, no differences in blood vessel density were detected in untreated and IMQ-treated animals of either genotypes, although a significant increase in blood vessel volume in IMQ-treated $E1^{+/+}$ animals was measured (Fig. 3).

EMILIN-1 deficiency favors the recruitment of macrophages in skin

IMQ-treated $E1^{-/-}$ mice showed a more pronounced inflammatory infiltrate compared to $E1^{+/+}$ mice (Fig. 4a). Immunostaining for CD45, Gr-1, and F4/80 was also informative: in fact, when we compared untreated and IMQ-treated $E1^{+/+}$ mice a significant increase in Gr-1 positive and to a lesser extent of F4/80 positive cells was detected (Fig. 4b and Supplemental Fig. 4a). This increase was not so evident for F4/80 positive cells in treated versus untreated $E1^{-/-}$ mice since there were significantly more F4/80 positive cells in $E1^{-/-}$ than in $E1^{+/+}$ mice both before and after IMQ treatment (Fig. 4b, c). This finding most likely indicates that the absence of EMILIN-1 induces an inflammatory state which promotes chronicity and exacerbation of the diseased tissue. The higher expression of Iba1, a macrophage marker, in skin tissue confirmed the association between EMILIN-1 deficiency and the higher numbers of macrophages already in the absence of any previous inflammatory stimulus (Fig. 4d). To strengthen the above finding and in order to simulate more closely a chronic inflammatory state as in human psoriasis, mice of the two genotypes were subjected to a "chronic" IMQ treatment and the skin was examined for Iba1 expression. Also under this treatment $E1^{-/-}$ mice demonstrated that the area positive for Iba1 was twice larger than in $E1^{+/+}$ mice (Supplemental Fig. 4b). In general, the promotion of an immune infiltrate was likely not due to a differential increase in cell death, as indicated by the statistically not significant differences in the number of apoptotic cells in the skin of untreated and IMQ-treated $E1^{+/+}$ and $E1^{-/-}$ mice, as assessed by TUNEL assays (Supplemental Fig. 4c, d).

To test whether not only the absence of EMILIN-1 but also its alterations were sufficient to induce a more severe inflammatory state, IMQ treatment was also applied to E1-E933A transgenic (E933A TG) mice, which express an EMILIN-1 protein carrying a mutation in the gC1q residues involved in the interaction with the α4/α9 integrins [13,29]. Macroscopically, the E933A TG mice showed less severe skin inflammation than $E1^{-/-}$ mice in terms of classic signs of psoriasis such as erythema and scaling (Supplemental Fig. 5a). Compared with WT mice, E933A TG mice exhibited a more pronounced inflammation after IMQ treatment, with numbers of CD45- and Gr-1-positive cells very similar to those of $E1^{-/-}$ mice (Supplemental Fig. 5b). If compared with $E1^{+/+}$ and $E1^{-/-}$ mice, after IMQ treatment the differences in the inflammatory cell infiltrate were not statistically significant. The basal number of CD45-, Gr-1-, and F4/80-positive cells in E933A TG mice was very close to that of $E1^{+/+}$ mice (Supplemental Fig. 5b), suggesting that the changes in the gC1q domain are not sufficient to promote an inflammatory environment in the absence of specific stimuli, as occurs in the absence of the whole EMILIN-1 molecule. Of note, the thickness of the epidermis of untreated E933A TG mice was comparable to that of $E1^{-/-}$ mice and significantly higher than that of $E1^{+/+}$ mice (Supplemental Fig. 5b).

Emilin1$^{-/-}$ dermal fibroblasts show a myofibroblastic phenotype

It is known that differentiation of fibroblasts into myofibroblasts, usually occurring in diseased tissues, can promote chronic and fibrotic alteration of the skin homeostasis [33]. To test whether the absence of EMILIN-1 could affect the dermal fibroblast phenotype, we first determined the presence of α-SMA-positive cells, i.e. myofibroblasts, in untreated and IMQ-treated mouse skins. The number of α-SMA-positive cells was significantly higher in $E1^{-/-}$ mice and the IMQ treatment did not induce any significant change (Fig. 5). Accordingly,

IMQ-treated animals. Three calculations for each field (x10 magnification) (at least 3 field for each mouse) were made to obtain the mean value. The results reported in the column graphs represent the mean ± SD of $n = 5-8$ mice. (e) H&E staining of FFPE sections of untreated and IMQ-treated mouse skin. Arrowheads indicate regions of fibroblast proliferation associated with focal epidermal hyperplasia. Arrows point the presence of Munro's abscesses in IMQ-treated $E1^{-/-}$ mice. The quantification of Munro's abscesses in $E1^{+/+}$and $E1^{-/-}$ mice following IMQ treatment is reported in the graph. Scale bars, 100 μm (c), 50 μm (e). *$P < 0.05$; **$P < 0.01$.

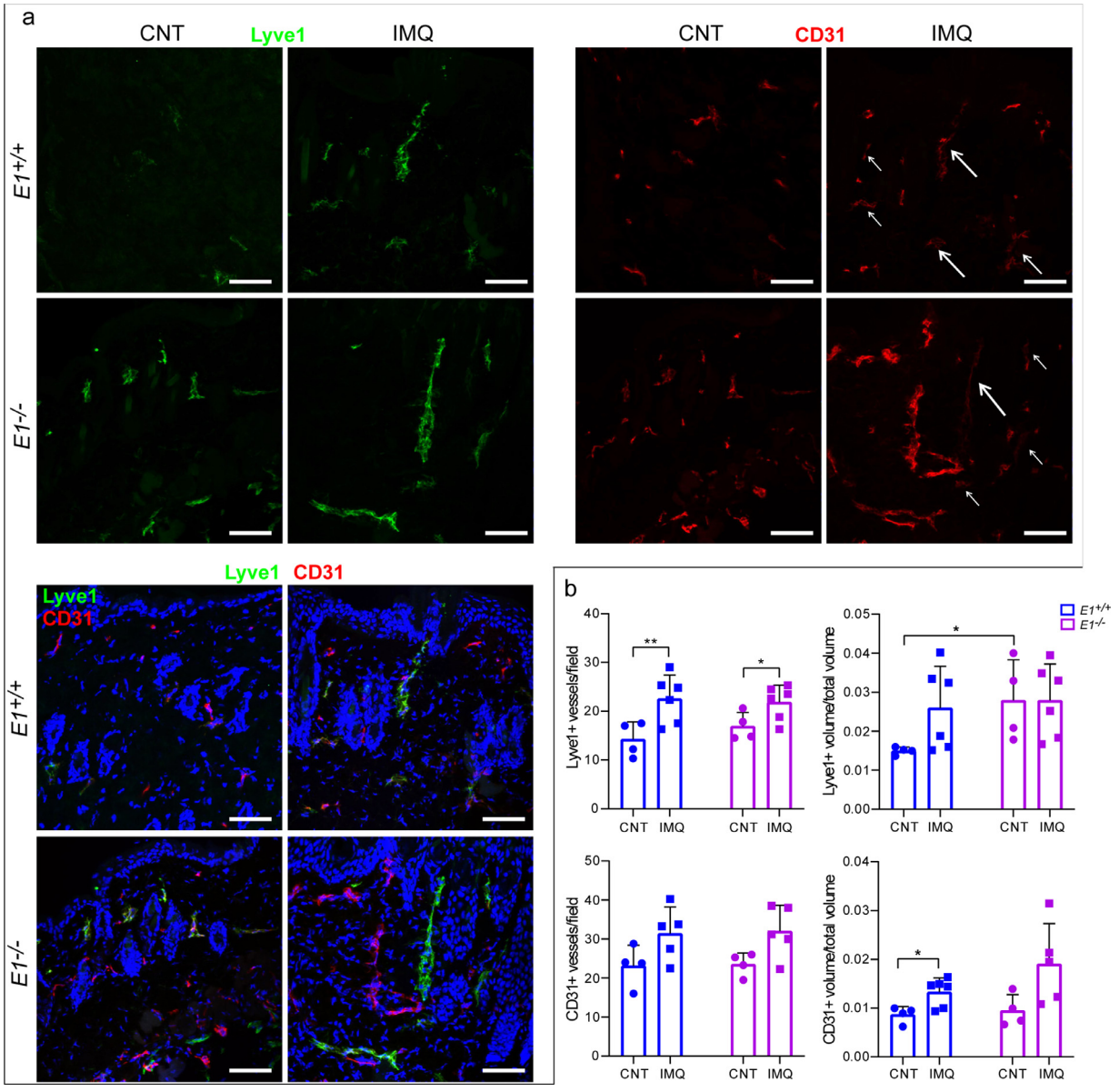

Fig. 3. Dermal LVs in $E1^{-/-}$ mice displayed morphological alterations also in the absence of a psoriatic stimulus. (a) Immunostaining of Lyve1 (green) and CD31 (red) positive vessels in untreated and IMQ-treated $E1^{+/+}$ and $E1^{-/-}$ mice. Cell nuclei are pseudocolored blue. Newly formed lymphatic vessels (IMQ-treated mice) display a high intense Lyve1 staining. White arrows indicate vessels with high Lyve1 and low CD31 positivity. (b) Quantification of positive vessels is shown as both number and volume of Lyve1- and CD31-positive vessels. At least four fields (x20 magnification) were analyzed to obtain a mean value for each mouse, and each point represents a single mouse. The results reported in the column graph represent the mean ± SD of $n = 4–6$ mice. Scale bar, 50 μm. $^{*}P < 0.05$; $^{**}P < 0.01$. (For interpretation of the references to color in this figure legend, the reader is referred to the web version of this article.)

fibroblasts isolated from $E1^{-/-}$ newborn mice expressed higher levels of α-SMA than $E1^{+/+}$ fibroblasts, suggesting a suppressive role exerted by EMILIN-1 in myofibroblast differentiation (Fig. 6a). Consequently, *Emilin1* silencing induced a myofibroblastic phenotype (Fig. 6b). Fibroblasts isolated from E933A TG newborn mice showed a slight but not significant increase in the levels of α-SMA (Fig. 6a). Since EMILIN-1 affects TGFβ maturation and, as a consequence, higher expression of the active form can be detected in $E1^{-/-}$ mice [13,18], we hypothesized that increased levels of the profibrotic cytokine [34] could be responsible for triggering myofibroblast differentiation. The treatment of fibroblasts with the TGFβ RI inhibitor LY364947 fully rescued the basal α-SMA staining in $E1^{+/+}$ fibroblasts even in the presence of recombinant TGFβ (Fig. 6c). In contrast, in $E1^{-/-}$ fibroblasts either in the absence or in the

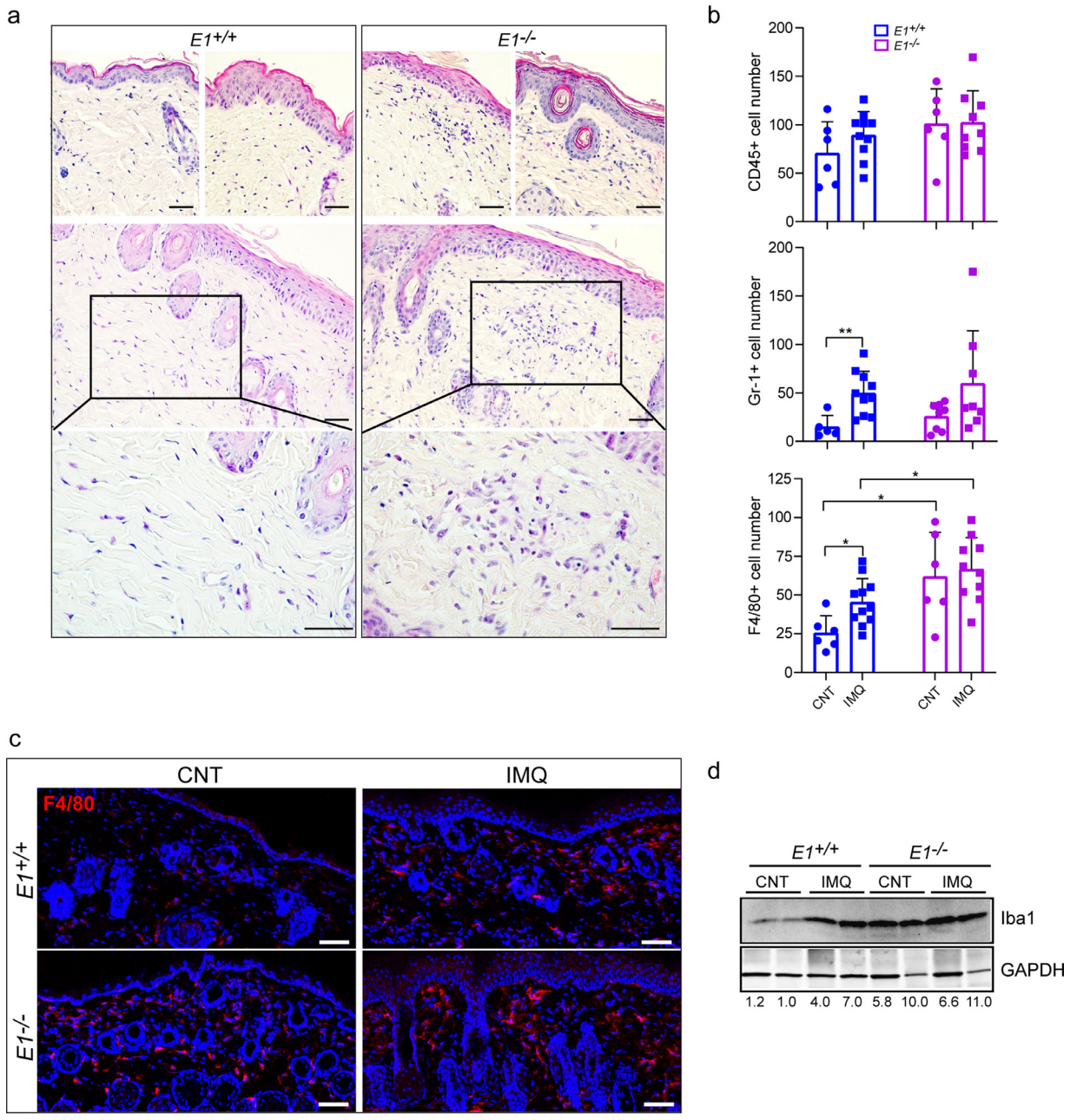

Fig. 4. EMILIN-1 deficiency favors the recruitment of macrophages in skin. (a) H&E staining of FFPE skin sections from IMQ-treated mice. Representative images of 3 mice for each genotype are shown. A more abundant and evident infiltrate (see magnification of the boxed region in the lower panel) characterizes $E1^{-/-}$ treated skin. (b) Quantification and characterization of the inflammatory infiltrate in cryostat skin sections immunostained for CD45, Gr-1 and F4/80 markers. At least five fields (x20 magnification) were analyzed to obtain a mean value for each mouse. The results reported in the column graphs represent the mean ± SD of $n = 6-10$ mice. (c) Representative immunofluorescence images for the detection of F4/80 positive cells in cryostat sections of untreated and IMQ-treated skin. (d) Immunoblot of the Iba1 protein level in untreated and IMQ-treated skin from $E1^{+/+}$ and $E1^{-/-}$ mice. Two samples for each genotype and treatment are shown. Quantitative measurements of Iba1 protein levels, normalized using GAPDH as loading control, are reported for each sample. Scale bar, 50 μm. $^{*}P < 0.05$; $^{**}P < 0.01$.

presence of exogenous TGFβ, the inhibitor only partially reduced α-SMA expression (Fig. 6c). These results were consistent with alterations of the TGFβ signaling pathway. Consequently, $E1^{-/-}$ fibroblasts displayed augmented levels of pSmad and pErk (Fig. 6d). In addition, we also found increased

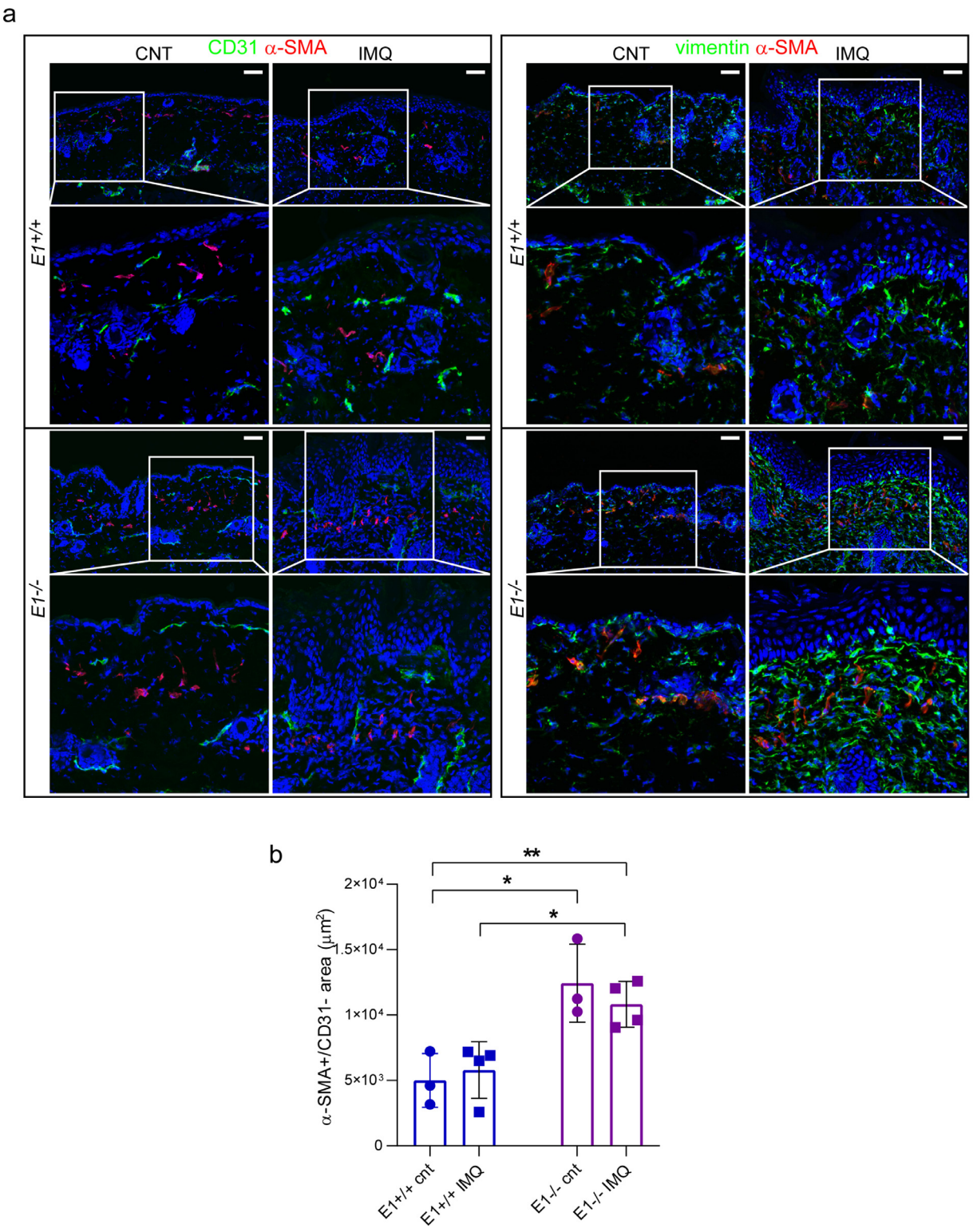

Fig. 5. $E1^{-/-}$ dermal fibroblasts show an activated phenotype. (a) CD31 (green)/α-SMA (red) (left) and vimentin (green)/α-SMA (red) (right) staining of cryostat sections of untreated and IMQ-treated skins from $E1^{+/+}$ and $E1^{-/-}$ mice. Nuclei are pseudocolored in blue. A magnification of each representative image is reported in the boxed area. (b) Quantification of α-SMA-positive/CD31-negative areas are reported in the graph. Mean values were obtained through the analysis of at least four fields (x20 magnification) for each mouse; points represent the values of a single mouse. The results reported in the column graph represent the mean ± SD of $n = 3-4$ mice. Scale bar, 50 μm. $^{*}P < 0.05$; $^{**}P < 0.01$. (For interpretation of the references to color in this figure legend, the reader is referred to the web version of this article.)

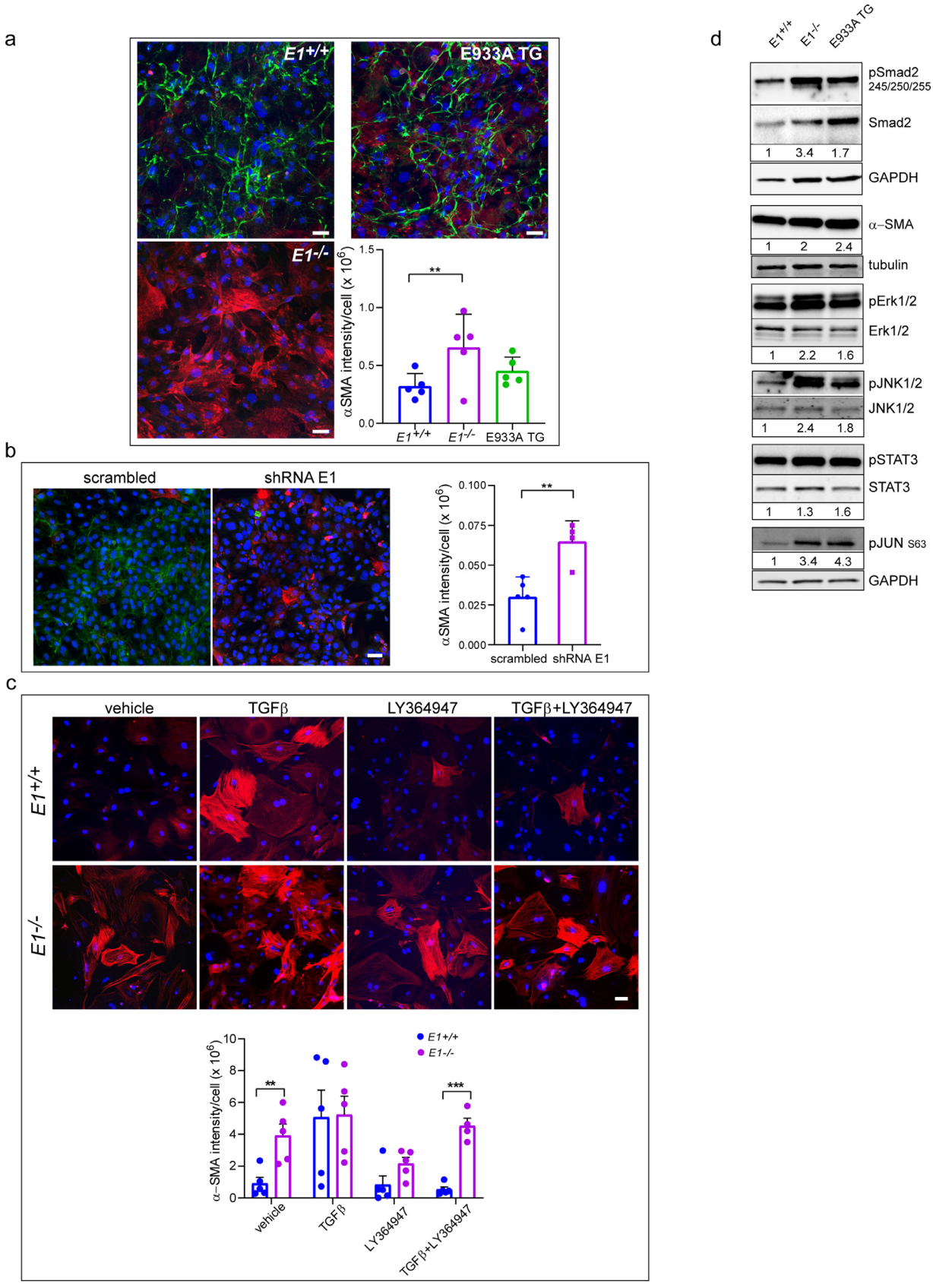

Fig. 6. *E1*$^{-/-}$ fibroblasts show a myofibroblastic phenotype. (a) Representative images of fibroblasts isolated from newborn *E1*$^{+/+}$, *E1*$^{-/-}$ and E933A TG mice and stained for EMILIN-1 (green) and α-SMA (red). (b) Representative images of NIH 3T3 fibroblasts silenced (shRNA E1) or not (scrambled) for EMILIN-1 expression and stained for EMILIN-1 (green)

phosphorylation of JNK and JUN in $E1^{-/-}$ fibroblasts, consistent with a pronounced non-canonical activation of TGFβ (Fig. 6d) [35]. To test whether the activated phenotype was solely due to dysregulation of TGFβ or whether the loss of integrin engagement by EMILIN-1 could also play a role, we used fibroblasts isolated from E933A TG mice. This mutant is still capable to bind pro-TGFβ through the EMI domain. The levels of α-SMA and pSTAT3 as well as the levels of pErk, pJNK, and pJUN in E933A TG fibroblasts were slightly higher than in $E1^{+/+}$ fibroblasts, suggesting that signaling regulated by the interaction between gC1q and integrin may also affect TGFβ pathway in these cells (Fig. 6a, d). We then incubated murine fibroblasts of the three genotypes ($E1^{+/+}$, $E1^{-/-}$, E933A TG) with soluble gC1q and examined the changes in α-SMA staining. Although not statistically significant, the addition of gC1q reduced the intensity of α-SMA staining and partially rescued the effect caused by TGFβ signaling alterations in $E1^{-/-}$ and NIH-3T3 silenced fibroblasts (Fig. 7a). Nonetheless, the treatment with recombinant gC1q induced a significant decrease of α-SMA staining in E933A TG fibroblasts (Fig. 7a). On the contrary, $E1^{+/+}$ fibroblasts were insensitive to the addition of exogenous gC1q most likely since endogenously secreted EMILIN-1 can already engage the integrin receptors. Importantly, the use of the function-blocking anti-gC1q antibody (1H2) was able to reduce the effect in $E1^{-/-}$ fibroblasts, suggesting that the activity of gC1q on α-SMA was specific (Fig. 7b). The role played by the EMILIN-1/integrin interaction in this context was further demonstrated by the use of a function-blocking antibody against the α4 integrin subunit which abrogated the action of added gC1q both in $E1^{-/-}$ and E933A TG fibroblasts (Supplemental Fig. 6a). Moreover, the small increase in the number of myofibroblasts in E933A TG mice (Supplemental Fig. 6b) suggest that the interaction between gC1q and integrin may also exert an opposing, albeit weak, effect on myofibroblastic differentiation. The effect of the absence of EMILIN-1 and the consequent TGFβ dysregulation [18] were evident in $E1^{-/-}$ skin tissue characterized by a prominent collagen deposition (Supplemental Fig. 7a). In contrast, no evident fibrosis was observed in the skin of $E1^{+/+}$ mice; E933A TG mice displayed intermediate levels of collagen deposition (Supplemental Fig. 7a), consistent with the normal TGFβ levels detected in this mutant [29]. In agreement with these findings, the skin of $E1^{-/-}$ mice and to a lesser extent E933A TG mice displayed higher levels of Axl, a receptor tyrosine kinase implicated in fibrogenic signaling pathways involving myofibroblast activation [36,37] (Supplemental Fig. 7b). Analysis of skin tissues with a mouse cytokine array showed that protein levels of some markers of fibrosis were higher in $E1^{-/-}$ mice (Supplemental Fig. 7c).

Emilin1$^{-/-}$ dermal fibroblasts promote the recruitment of macrophages and their polarization toward a pro-inflammatory phenotype

Fibroblasts may exhibit either pro- or anti-inflammatory properties and influence leukocyte recruitment [38–40]. In particular, dermal fibroblasts play an important role in the inflammatory response in psoriasis by promoting the polarization of monocytic cells toward a pro-inflammatory condition [41]. First, to test whether EMILIN-1 deficiency in fibroblasts could affect macrophage chemotactic migration, RAW 264.7 monocytic cells were used in a Transwell-based motility assay in which conditioned media (CM) from resting or IL-1α-stimulated $E1^{+/+}$, $E1^{-/-}$ and E933A TG fibroblasts were added as chemoattractants. The CM from $E1^{-/-}$ fibroblasts induced a slightly higher monocyte motility compared with that from $E1^{+/+}$fibroblasts (Fig. 8a). This effect was even more pronounced when fibroblasts were pre-stimulated with IL-1α (Fig. 8a). Analysis of skin tissues with a mouse cytokine array also showed that protein levels of factors able to recruit monocytic cells were higher in $E1^{-/-}$ mice (Fig. 8b). Then, to verify if the loss of EMILIN-1 in fibroblasts could in turn affect macrophage polarization, RAW 264.7 cells were challenged with the CM, and the expression of the M1 marker TNFα and M2 marker IL-10 assessed. Macrophages treated with CM from $E1^{-/-}$ fibroblasts expressed more TNFα than those incubated with $E1^{+/+}$ fibroblasts CM; on the other hand, a much higher expression of IL-10 was detected when using CM from $E1^{+/+}$ fibroblasts (Fig. 8c). The CM from E933A TG fibroblasts induced the same effects, albeit less pronounced, on macrophages as the CM from $E1^{-/-}$ fibroblasts (Fig. 8c). RAW 264.7 cells treated with CM from

and α-SMA (red). (c) $E1^{+/+}$ and $E1^{-/-}$ fibroblasts were treated for 24 h with TGFβ with or without the TGFβ RI inhibitor (LY364947) and then stained for α-SMA (red). The corresponding quantification of α-SMA intensity per cell is shown in the graphs (a–c). Nuclei are pseudocolored in blue (a-c). At least five fields (x20 magnification) were analyzed to obtain the mean value for each experiment. The results reported in the column graphs (b, c and d) represent the mean ± SD of $n = 5$ experiments. Scale bar, 50 μm. $^{**}P < 0.01$, $^{***}P < 0.001$. (d) Western blotting analyses for pJNK, pSMAD, pERK, pSTAT3 and pJUN and α-SMA in cellular lysates obtained from $E1^{+/+}$, $E1^{-/-}$ and E933A TG newborn fibroblasts. The signal of phosphorylated proteins was normalized to the respective total protein or to housekeeping proteins (GAPDH, tubulin). (For interpretation of the references to color in this figure legend, the reader is referred to the web version of this article.)

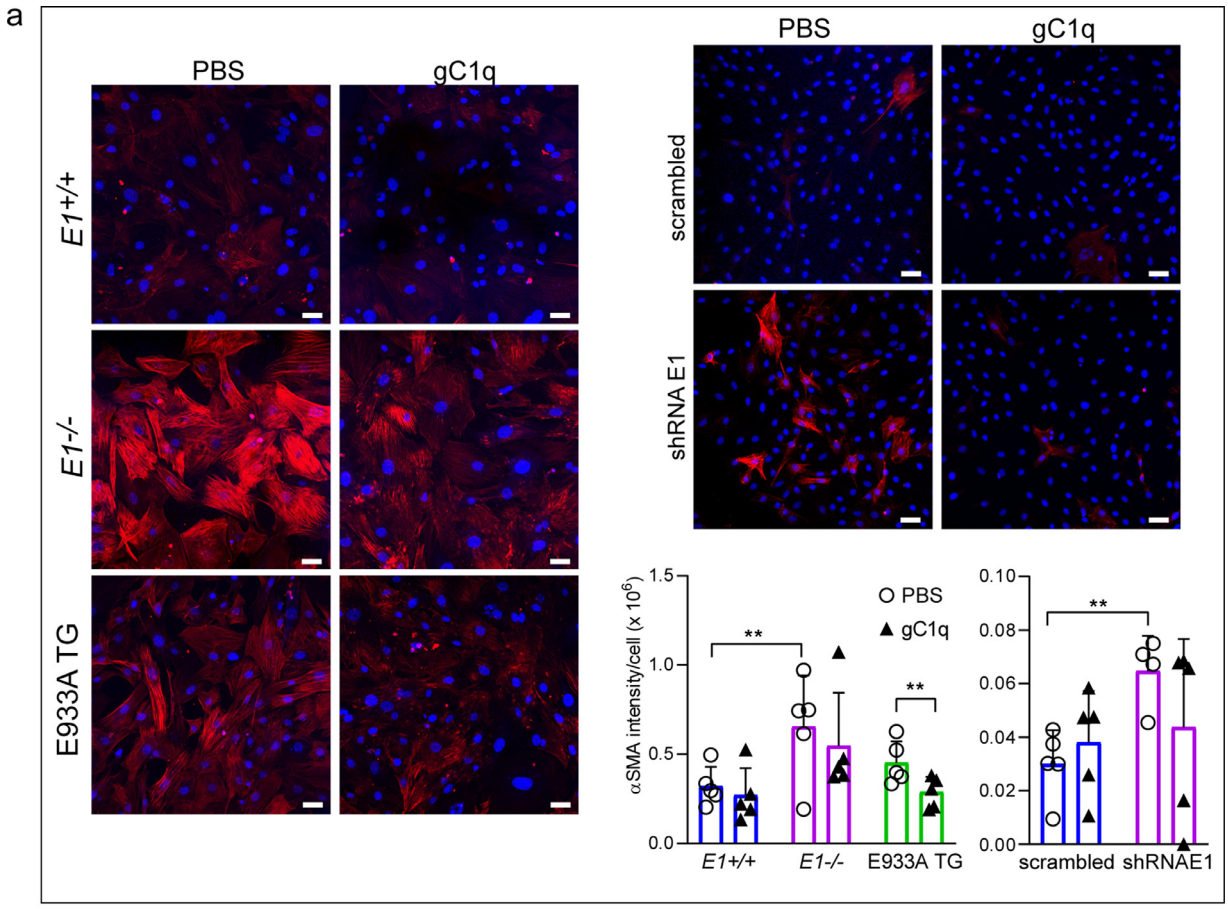

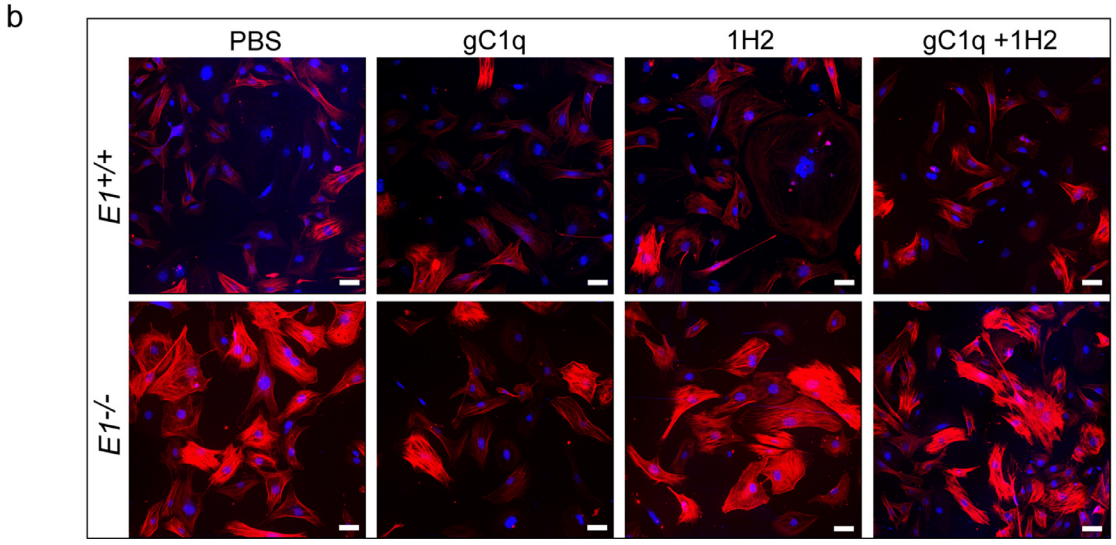

Fig. 7. gC1q domain partially regulates myofibroblast differentiation. (a) Representative images of $E1^{+/+}$, $E1^{-/-}$, E933A TG, scrambled and shRNAE1 NIH 3T3 fibroblasts treated with gC1q for 48 h and then stained for α-SMA (red). The corresponding quantification of α-SMA intensity per cell is shown in the graphs. At least five fields (x20 magnification) were analyzed to obtain a mean value for each experiment. The results reported in the column graphs represent the mean ± SD of $n = 5$ experiments. (b) Representative images of $E1^{+/+}$ and $E1^{-/-}$ fibroblasts treated with gC1q in the presence or absence of the gC1q function blocking antibody 1H2 for 48 h and then stained for α-SMA (red). Scale bar, 50 μm. $^{**}P < 0.01$. (For interpretation of the references to color in this figure legend, the reader is referred to the web version of this article.)

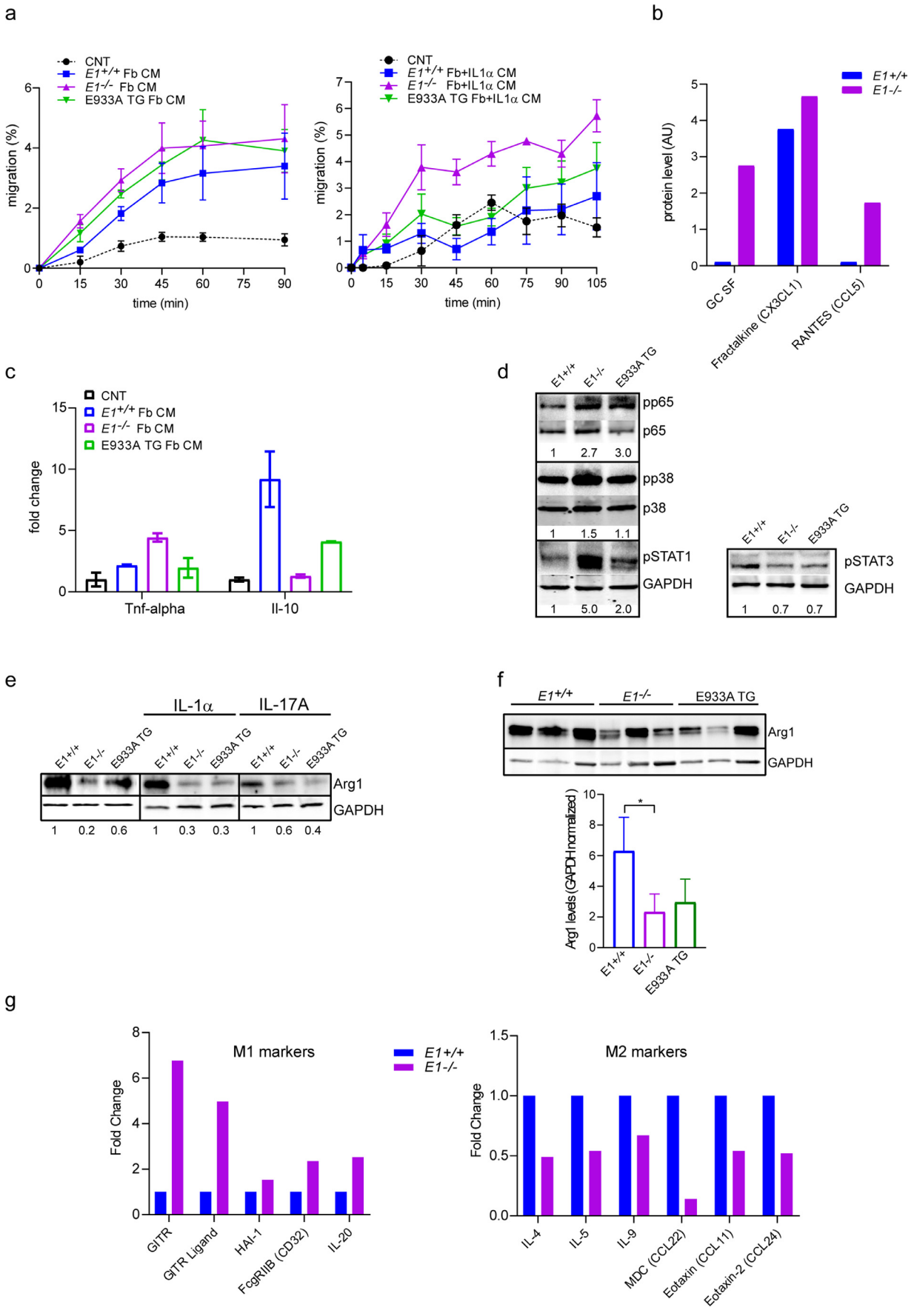

Fig. 8. *E1*$^{-/-}$ fibroblasts induce macrophage chemotaxis and polarization to a pro-inflammatory phenotype. (a) Chemotactic migration of RAW 264.7 monocytic cells induced by conditioned medium (CM) derived from resting (left) or IL-1α-

E1$^{-/-}$ or E933A TG fibroblasts exhibited activation of p65, p38, and STAT1, known to be involved in the transcription of M1 genes [42]. Accordingly, lower levels of pSTAT3, which induces the transcription of M2 genes [42] were detected (Fig. 8d). RAW 264.7 cells were also incubated with CM from fibroblasts stimulated with IL-1α or IL-17A, two known mediators of psoriasis. Also in this case, the levels of the M2 marker Arg1 were increased after treatment with CM from resting or IL-1α/IL-17A-stimulated *E1*$^{+/+}$ fibroblasts (Fig. 8e). Similarly, the levels of Arg1 were higher in *E1*$^{+/+}$untreated skin compared to those determined in *E1*$^{-/-}$ and E933A TG animals (Fig. 8f). The levels of M1 and M2 markers analyzed in the skin tissues were, respectively, higher and lower in *E1*$^{-/-}$ mice compared to *E1*$^{+/+}$ mice, supporting the finding that the pro-inflammatory phenotype was already pronounced in the absence of EMILIN-1 before treatment in the resting state (Fig. 8g). Taken together these results indicate that the lack and/or the reduction of EMILIN-1 did not only promote LV proliferation but also led to a persistent pro-inflammatory state.

Discussion

In this study, we demonstrated that changes in EMILIN-1 state may alter the inflammatory context in skin, and ultimately drive macrophage polarization, leading to an imbalance in tissue homeostasis, thus generating a favorable environment for further disease development. The increased disease severity in IMQ-treated *E1*$^{-/-}$ mice was primarily due to a microenvironment more prone to the effects of acute inflammatory stimuli and subjected to the induction of chronic inflammation. The analyses performed on the E933A TG mouse model gave us the opportunity to dissect the role of the EMI and gC1q domains of EMILIN-1 in the regulation of TGFβ and α4/α9 integrins and their contribution to inflammatory condition of psoriatic skin. We have previously demonstrated that EMILIN-1 fragmentation leads to a condition similar to that of *E1*$^{-/-}$ mice in which the glycoprotein is fully ablated, resulting in uncontrolled cell proliferation and abnormal lymphatic phenotype [27,31,32]. Therefore, we hypothesized that the digestion of EMILIN-1 by proteolytic enzymes released by inflammatory cells may represent a pathogenic mechanism leading to the decrease or loss of functions associated with the gC1q and/or EMI functional domains. Compared to healthy subjects, the expression of EMILIN-1 was significantly reduced in all psoriatic patients enrolled in this study. The finding that patients affected by psoriasis display normal EMILIN-1 mRNA levels and elevated expression of MMPs mRNA suggests that the glycoprotein could be extensively processed during the establishment of this disease. The presence of dilated podoplanin-positive vessels in psoriasis patients with a very low association to EMILIN-1, which has been shown to be a structural and functional regulator of LVs [23,29], indicates that the chronic inflammation characterizing this skin disease may be due to a very complex cellular and extracellular mechanistic network. This finding suggests that inflammatory environment may depend on increased TGFβ signaling resulting from the loss of the buffering EMILIN-1 activity. It is conceivable that during chronic skin disease molecular mechanisms are engaged to attenuate the ECM buffering function on TGFβ signaling, such as through the dismantlement of proteins like EMILIN-1.

In our animal models we were able to reproduce most of the typical aspects of psoriasis, and showed that *E1*$^{-/-}$ mice, and, to a lower macroscopic evidence, E933A TG mice developed more severe disease after IMQ treatment compared to *E1*$^{+/+}$ mice. *E1*$^{-/-}$ mice displayed a higher number of F4/80 positive cells already without treatment, suggesting that alterations of this ECM molecule may induce changes in the microenvironment associated with a pro-inflammatory disease development.

The higher presence of skin fibroblasts in *E1*$^{-/-}$ mice, which are responsible for a more severe fibrotic milieu as indicated by the marked collagen deposition and the increased levels of the markers of fibrosis, was mainly due to increased TGFβ

stimulated (right) *E1*$^{+/+}$, *E1*$^{-/-}$, and E933A TG fibroblasts. (b) Protein level of factors involved in the recruitment of monocytes/macrophages in *E1*$^{+/+}$and *E1*$^{-/-}$ untreated mice, as detected by the Mouse Cytokine Array C kit. Quantified tissue skin lysates from 3 animals were pooled and equal amounts of total protein were loaded onto the array membranes. The acquired images of the resulting dot blots were analyzed using ImageLab software. (c) RAW 264.7 cells were incubated for 48 h with CM obtained from *E1*$^{+/+}$, *E1*$^{-/-}$, and E933A TG fibroblasts. TNFα and IL-10 were analyzed as macrophage polarization markers by qPCR. (d) Representative immunoblot image of phosphorylated p65, p38, STAT1 and STAT3 levels in RAW 264.7 cells, incubated for 48 h with CM from resting *E1*$^{+/+}$, *E1*$^{-/-}$, and E933A TG fibroblasts. Quantitative measurements of protein levels, normalized using the total protein or GAPDH as loading control, are reported for each sample. (e) Representative immunoblot image of the Arg1 levels in RAW 264.7 cells, incubated for 48 h with CM from resting or IL-1α (1 ng/ml)/IL-17A (5 ng/ml) stimulated *E1*$^{+/+}$, *E1*$^{-/-}$, and E933A TG fibroblasts. Quantitative measurements of Arg1 protein levels, normalized using GAPDH as loading control, are reported for each sample. (f) Arg1 levels in *E1*$^{+/+}$, *E1*$^{-/-}$, E933A TG skin tissues from different animals. Quantification was reported in the graph as mean ± SD (n = 3). (g) Fold change of the levels of M1 and M2 polarization markers detected in untreated *E1*$^{+/+}$and *E1*$^{-/-}$ mice using the Mouse Cytokine Array C kit as reported in (b).

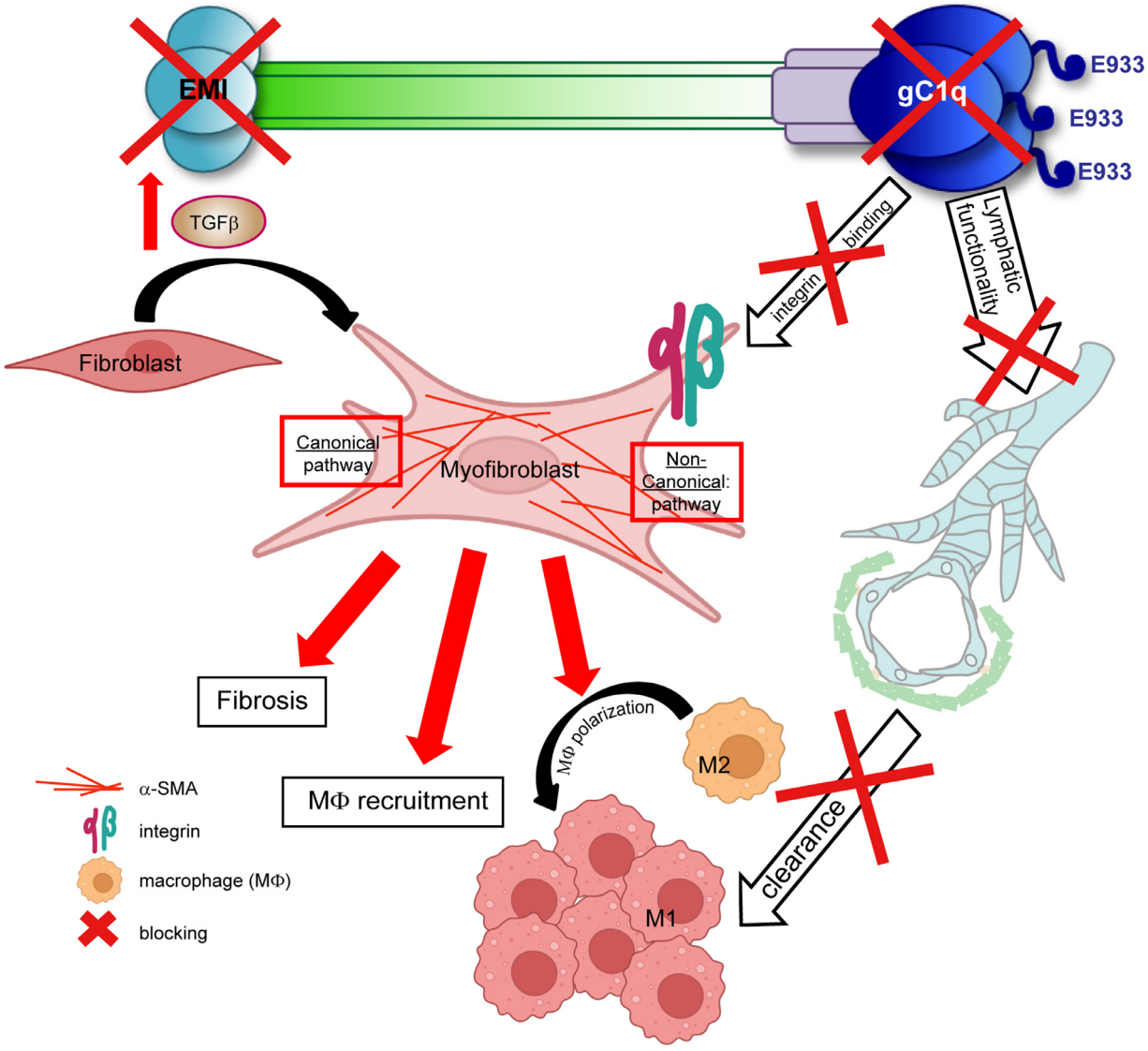

Fig. 9. Proposed model for the role of EMILIN-1 in chronic disease. The illustration summarizes the proposed molecular mechanisms by which EMILIN-1 loss might alter the inflammatory context in the skin. The induction of a myofibroblastic phenotype, which recruits monocytes, drives macrophage polarization toward M1-type cells, and promotes fibrosis, is due on one side to the increased levels of mature TGFβ in the absence of the EMI domain that prevents its maturation in the extracellular space, as is the case of the *E1*$^{-/-}$ mouse model. On the other side, the lack of integrin-specific binding by the gC1q domain mutated in the E933A TG mouse model or completely absent in *E1*$^{-/-}$ mice also drives alterations in the non-canonical signaling pathway of TGFβ, and favors the switch to a myofibroblast phenotype. Furthermore, by acting on lymphatic vessel structure and function, gC1q may alter the clearance of inflammatory infiltrates, supporting a final imbalance in skin homeostasis and creating a favorable environment for disease development.

signaling upon EMILIN-1 loss, as previously shown by others [43–47]. More importantly, one of the most relevant changes observed in the null or mutated EMILIN-1 background was the induction of a myofibroblast phenotype capable to drive macrophage towards the M1 phenotype which in turn expresses also higher levels of VEGFC. These results are in line with emerging evidence supporting the recruitment and activation of macrophages in M1 subtype as determinant factors in human psoriasis [48,49]. A growing amount of evidences indicate that, depending on their location and soluble factors available, fibroblasts may exhibit either pro- or anti-inflammatory properties and influence leukocyte recruitment [38–40]. The results reported in this study reinforce the concept that fibroblasts/myofibroblasts are key cellular players in the context of skin disease; not only are they responsible for the synthesis and likely the remodeling of EMILIN-1, a crucial regulator of skin homeostasis [20], but can also

affect macrophage polarization thus profoundly altering the microenvironment.

Our results indicate that EMILIN-1 can affect the inflammatory response through different mechanisms hinging on both the EMI and gC1q domains. A model summarizing how EMILIN-1 may alter the inflammatory environment of skin is shown in Fig. 9. Notably, we suggest that the dismantlement of the EMI domain of EMILIN-1 by proteolysis may lead to the up-regulation of TGFβ which promoted the differentiation of fibroblasts into myofibroblasts. As a consequence the release of soluble factors by these cells polarized macrophages toward the M1 phenotype thus leading to the establishment of a chronic inflammatory milieu. The abnormal and complex dysregulation of TGFβ caused by EMILIN-1 deficiency with the activation of both canonical and non-canonical pathway was already described in a model of aortic valve disease [45]. In the present study we provide evidence that also the gC1q domain can affect TGFβ signaling; thus, the gC1q domain displays a dual function in the context of psoriasis, through the interaction with keratinocytes and fibroblasts it controls skin homeostasis [20,25], whereas through the stimulation of non-canonical TGFβ signaling it alters the microenvironment and impinges on inflammation, as demonstrated by the E933A TG mouse model. Furthermore, our results suggest that the more consistent inflammatory response upon IMQ treatment of *E1*$^{-/-}$ and E933A TG mice could also be due to structural as well as functional lymphatic dysregulation. The analyses of psoriasis patients, in which lower levels of EMILIN-1 were present with a very rare association with LVs, highlight the multifaceted role of this ECM component in the skin inflammatory scenario.

In conclusion, this study supports the evidence that the ECM not only exerts purely mechanical properties, including stability and guidance for cell movement, or serves as a reservoir for growth factors, but also modulates cell functions. Uncovering the role of the ECM in influencing the inflammatory response is a promising area of research. Our results highlight for the first time the important role of EMILIN-1 in regulating macrophage recruitment and polarization and provide a new perspective for delineating the complex network in inflammatory diseases.

Materials and methods

Patients

Skin biopsies were obtained from psoriatic lesions of 13 patients at Santo Andrea Hospital (Rome, Italy), where written informed consent was obtained. Experienced dermatologists and pathologists classified the lesions as psoriasis according to histopathological diagnostic criteria. Patients were of both sexes (7 males and 6 females) and similar age (54±18 and 54±9 years old, respectively). The control samples of healthy skin were age-matched.

Chemicals and reagents

Recombinant TGFβ protein was purchased from Peprotech (London, UK). The TGFβRI inhibitor LY364947 was purchased from Calbiochem (Merk, Germany). Recombinant gC1q molecule was prepared and purified as previously described [22]. Commercial primary antibodies used for Western blot and immunofluorescence are listed in Table S1. Mouse anti gC1q (clone 1H2) and rabbit anti EMILIN1 (As556) antibodies were produced in our laboratory as previously described [22].

Primary cells and cell lines

Murine dermal fibroblasts were isolated as previously described [50]. Briefly, sterile newborn skin was incubated overnight at 4 °C in 0.25% trypsin solution without EDTA (Lonza). Dermis was digested with collagenase-dispase solution (Roche) for 30 min at 37 °C followed by DNAse (Roche) for 10 min. Dermal samples were diluted with medium, passed through cell strainers to remove undigested skin fragments and centrifuged at 150 g for 5 min. Pellets and supernatants were resuspended and centrifuged according to the original protocol. Established fibroblast cultures were maintained in Dulbecco Modified Eagle Medium (DMEM, GIBCO) supplemented with L-Glutamine (GIBCO), 10% fetal bovine serum (FCS, GIBCO) and antibiotics (10,000 U/ml penicillin and 10 mg/ml streptomycin). NIH 3T3 and RAW 264.7 cells were obtained from ATCC and were cultured, respectively in low glucose DMEM and high glucose DMEM both supplemented with 10% FCS and antibiotics. NIH 3T3 cells silenced for *Emilin1* were established as previously described [20], and maintained in DMEM supplemented with 10% FCS, antibiotics and 1 μg/ml puromycin (Sigma).

Chemotaxis assay

Migration was performed on Transwell-like inserts with fluorescence-shielding porous PET membranes (polycarbonate-like material with 8 μm pores) HTS FluoroBlok™ inserts (Becton-Dickinson, Falcon), as previously described [51]. Conditioned media derived from primary fibroblasts isolated from *E1*$^{+/+}$, *E1*$^{-/-}$ and E933A TG mice and cultured for 24 h in the presence of DMEM containing 2% FCS or after 24 h of stimulation with IL-1α (1 ng/ml) were used as chemoattractants. Supernatants were then centrifuged and stored at −80 °C until use. RAW 264.7

cells were fluorescently tagged with the lipophilic dye FastDiI (Molecular Probes) at the final concentration of 5 μg/ml for 10−15 min at 37 °C. Cells were added to the top of the inserts (1.5×10^5 cells/insert). Control medium (DMEM supplemented with 2% FCS) or conditioned medium derived from 2×10^5 fibroblasts was added to the lower chamber. Cell migration was monitored at different time intervals by independent fluorescence detection from the top (corresponding to *non-migrated cells*) and the bottom (corresponding to *migrated cells*) side of the membrane using the computerized Infinite M1000 microplate reader (TECAN).

RT-PCR analysis

Total RNA was extracted using NucleoSpin RNA II (Macherey-Nagel, Germany) according to the manufacturer's instructions and the concentration was determined using a spectrophotometer (NanoDrop ND-1000, Thermofisher). Reverse transcription was performed using 1 μg of total RNA. The cDNA products were amplified using iQ SYBR Green Supermix (Bio-Rad Laboratories, Italy) with the following primers: Tnf-alpha **F** GTA GCC CAC GTC GTA GCA AA **R** ACA AGG TAC AAC CCA TCG GC; Il10 **F** CTG AAG ACC CTC AGG ATG CG **R** ACA CCT TGG TCT TGG AGC TTA T; Gapdh **F** AGG TCG GTG TGA ACG GAT TTG **R** TGT AGA CCA TGT AGT TGA GGT CA. qRT-PCR were performed using CFX96 qPCR (Bio-Rad) and data were analyzed with dedicated software CFX Maestro (Bio-Rad).

IMQ-induced mouse model of psoriasis

C57Bl/6 mice were purchased from Charles River Laboratories. *Emilin1*$^{-/-}$ (*E1*$^{-/-}$) and E933A TG mice (C57Bl/6 background) were generated as previously described [28]. All animal procedures and their care were performed according to the Institutional guidelines, in compliance with national laws and authorization by the Italian Ministry of Health to Dr. Spessotto (no. 632/2020). 8 week-old male *E1*$^{+/+}$, *E1*$^{-/-}$ and E933A TG mice received a daily topical dose of 62.5 mg of the IMQ cream (5%) (Imunocare; DFA Cooper SpA) on the shaved backs as shown in Fig. 2a. The control *E1*$^{+/+}$, *E1*$^{-/-}$ and E933A TG group was treated with a control vehicle (vaseline) cream. Mice were sacrificed by CO_2, and skin samples were collected.

Histology of mouse tissues

Skin specimens from the back were embedded in OCT and snap frozen or fixed overnight in formalin and then embedded in paraffin (FFPE). For histological examination, 5 μm thick sections were stained with hematoxylin and eosin (H&E), and three to four images were taken for each sample using a light microscope (Leica DM750) equipped with a CCD camera and dedicated software (Las EZ Leica). ImageJ software (http://rsb.info.nih.gov) was used for measurements.

Immunofluorescence

To perform immunofluorescence, samples were pretreated as follows: cells were cultured on glass coverslips, fixed with 4% paraformaldehyde (PFA) for 10 min, permeabilized in 0.1% Triton X-100 (Sigma) for 5 min, and blocked with 2% FCS and 1% BSA (Sigma) for 1 h at room temperature (RT); mouse dorsal tissues were embedded in OCT, snap frozen, and cryostat sections were fixed with 4% PFA or ice-cold acetone and blocked with 5% normal serum in 1% BSA/PBS solution; human samples were fixed in formalin and embedded in paraffin (FFPE), deparaffinized three times for 10 min with xylene (Merck), rehydrated in graded ethanol solution (100% for 5 min, 95% for 5 min, 70% for 2 min), then subjected to heat-mediated antigen retrieval with citrate buffer pH 6.0 and blocked with 5% normal serum in 1% BSA/PBS solution. Samples were then incubated overnight at 4 °C in a humidified chamber with specific primary antibodies (see Table S1), followed by appropriate secondary antibodies for 1 h at RT. All solutions and washes were performed in PBS. Samples were counterstained with TO-PRO-3 (Invitrogen, Thermo Fisher Scientific) and mounted with glycerol-based antifade agent. Sections incubated with an antibody of the same isotype but with irrelevant specificity served as controls.

To quantitatively evaluate the infiltrate of inflammatory cells, series of images were acquired at 40 × magnification using a true confocal scanning system (TCS SP8 FSU AOBS, Leica Microsystems) equipped with a Leica DMi8 inverted microscope (Leica Microsystems). The maximum projections obtained were then processed using LAS software (Leica Microsystems) and the Volocity 3D image analysis software (PerkinElmer), and the CD45, F4/80, and Gr1 positive cells were counted in four to five fields by two independent researchers. To quantitatively assess EMILIN-1 status and skin vessel density, three to five series of images were acquired at 20 × magnification using a TCS SP8 FSU AOBS confocal scanner system (Leica Microsystems). The intensity of positive fluorescence from EMILIN-1, Lyve1, CD31 and α-SMA was quantified using the Volocity software (PerkinElmer).

Western blot analysis

Skin samples were snap frozen and stored at −80 °C until use. Skin samples were homogenized in lysis buffer using gentleMACS Dissociator (Miltenyi Biotech, Germany). Cells were lysed in RIPA

buffer. Cell debris were removed from the homogenates by centrifugation at 10,000 g for 20 min. Tissue and cell lysates were quantified using the Bradford assay (Bio-Rad). 40−80 mg of total lysates were loaded onto 4−20% SDS polyacrilamide gels (Criterion Precast Gel, BioRad) and transferred onto nitrocellulose membranes (Amersham Hybond-ECL, Amersham Pharmacia Biotech, UK). Membranes were blocked with the everyBlot Blocking Buffer (BioRad) 1:1 with TBS for 1 h and incubated overnight at 4 °C with primary antibodies. After washing, membranes were incubated with the appropriate secondary antibodies. Chemiluminescent signals were visualized using Chemidoc Touch Imaging System (BioRad), fluorescent signals were detected using Odyssey CLx Near-Infrared Fluorescence Imaging System (LI-COR, Germany).

Cytokine profile array

Mouse skin samples were stored at −80 °C until use and homogenized in lysis buffer purchased from RayBiotech (Norcross, GA, USA), using Stainless Steel Beads and the TissueLyser System (Qiagen). Removal of cell debris from the homogenates was obtained by centrifugation at 10,000 g for 20 min.

Tissue skin lysates were quantified by Bradford assay (Bio-Rad Laboratories, Milan, Italy). The cytokine profile was determined using the Mouse Cytokine Array C kit (RayBiotech), which allows to quantify a panel of the most common cytokines secreted during the inflammatory processes. The assay was performed according to the manufacturer's instructions. Briefly, quantified tissue skin lysates from 3 animals were pooled and equal amounts of total protein (600 mg) were loaded onto the array membranes. Dot blots were visualized using Chemidoc Touch Imaging System (Bio-Rad) and acquired images were analyzed using the ImageLab software (Bio-Rad).

Analysis of publicy available datasets of gene expression in psoriatic patients

Gene Expression Omnibus (GEO) dataset comprising 58 patients (GSE13355) was downloaded and analyzed via GEO2R (https://www.ncbi.nlm.nih.gov/geo/geo2r). Expression profiles of Emilin1 and MMPs in healthy subjects (n = 64) and in normal adjacent and psoriatic tissues from patients (n = 58) were further analyzed and plotted using GraphPad Prism v8 (GraphPad Software, san Diego,CA, USA). GSE11903, GSE14905, and GSE30999 were also downloaded and analyzed for Emilin1 expression.

Funding

This work was supported by the CRO Ricerca Corrente core grant (linea 1) from Ministero della Salute to PS. mmc1.docx

Declaration of Competing Interest

None.

Acknowledgmnt

We thank present and past members of the 3 M Lab for their valuable contributions. In particular we want to sincerely thank Professor Alfonso Colombatti for his suggestions, critical contribution and many general teachings.

Received 3 February 2022;
Received in revised form 16 June 2022;
Accepted 20 June 2022
Available online 25 June 2022

Keywords:
Inflammation;
Psoriasis;
Myofibroblast;
Macrophage;
Lymphatic vessel;
Integrin

[1]These authors share co-last authorship.

References

[1] E. Shimshoni, I. Adir, R. Afik, I. Solomonov, A. Shenoy, M. Adler, L. Puricelli, F. Sabino, S. Savickas, O. Mouhadeb, N. Gluck, S. Fishman, L. Werner, T.M. Salame, D.S. Shouval, C. Varol, U. Auf dem Keller, A. Podestà, T. Geiger, P. Milani, U. Alon, I. Sagi, Distinct extracellular-matrix remodeling events precede symptoms of inflammation, Matrix Biol. 96 (2021) 47–68, doi: 10.1016/j.matbio.2020.11.001.

[2] J. Herrera, C.A. Henke, P.B. Bitterman, Extracellular matrix as a driver of progressive fibrosis, J. Clin. Invest. 128 (2018) 45–53, doi: 10.1172/JCI93557.

[3] N.K. Karamanos, A.D. Theocharis, T. Neill, R.V. Iozzo, Matrix modeling and remodeling: a biological interplay regulating tissue homeostasis and diseases, Matrix Biol. (2018), doi: 10.1016/j.matbio.2018.08.007.

[4] R. Khokha, A. Murthy, A. Weiss, Metalloproteinases and their natural inhibitors in inflammation and immunity, Nat. Rev. Immunol. 13 (2013) 649–665, doi: 10.1038/nri3499.

[5] V. Caputo, C. Strafella, A. Termine, A. Dattola, S. Mazzilli, C. Lanna, T. Cosio, E. Campione, G. Novelli, E. Giardina, R. Cascella, Overview of the molecular determinants

contributing to the expression of psoriasis and psoriatic arthritis phenotypes, J. Cell. Mol. Med. (2020), doi: 10.1111/jcmm.15742.
[6] L. Sorokin, The impact of the extracellular matrix on inflammation, Nat. Rev. Immunol. 10 (2010) 712–723, doi: 10.1038/nri2852.
[7] W.H. Boehncke, M.P. Schön, Psoriasis, Lancet 386 (2015) 983–994, doi: 10.1016/S0140-6736(14)61909-7.
[8] R. Kunstfeld, S. Hirakawa, Y.K. Hong, V. Schacht, B. Lange-Asschenfeldt, P. Velasco, C. Lin, E. Fiebiger, X. Wei, Y. Wu, D. Hicklin, P. Bohlen, M. Detmar, Induction of cutaneous delayed-type hypersensitivity reactions in VEGF-A transgenic mice results in chronic skin inflammation associated with persistent lymphatic hyperplasia, Blood 104 (2004) 1048–1057, doi: 10.1182/blood-2003-08-2964.
[9] I.M. Braverman, J. Sibley, Role of the microcirculation in the treatment and pathogenesis of psoriasis, J. Invest. Dermatol. 78 (1982) 12–17, doi: 10.1111/1523-1747.ep12497850.
[10] A. Henno, S. Blacher, C.A. Lambert, C. Deroanne, A. Noël, C. Lapière, M. de la Brassinne, B.V. Nusgens, A. Colige, Histological and transcriptional study of angiogenesis and lymphangiogenesis in uninvolved skin, acute pinpoint lesions and established psoriasis plaques: an approach of vascular development chronology in psoriasis, J. Dermatol. Sci. 57 (2010) 162–169, doi: 10.1016/j.jdermsci.2009.12.006.
[11] K. Alitalo, T. Tammela, T.V. Petrova, Lymphangiogenesis in development and human disease, Nature 438 (2005) 946–953, doi: 10.1038/nature04480.
[12] S. Schwager, M. Detmar, Inflammation and lymphatic function, Front. Immunol. 10 (2019) 308, doi: 10.3389/fimmu.2019.00308.
[13] A. Capuano, E. Pivetta, G. Sartori, G. Bosisio, A. Favero, E. Cover, E. Andreuzzi, A. Colombatti, R. Cannizzaro, E. Scanziani, L. Minoli, F. Bucciotti, A.I. Amor Lopez, K. Gaspardo, R. Doliana, M. Mongiat, P. Spessotto, Abrogation of EMILIN1-β1 integrin interaction promotes experimental colitis and colon carcinogenesis, Matrix Biol. 83 (2019) 97–115, doi: 10.1016/j.matbio.2019.08.006.
[14] A. Hagura, J. Asai, K. Maruyama, H. Takenaka, S. Kinoshita, N. Katoh, The VEGF-C/VEGFR3 signaling pathway contributes to resolving chronic skin inflammation by activating lymphatic vessel function, J. Dermatol. Sci. 73 (2014) 135–141, doi: 10.1016/j.jdermsci.2013.10.006.
[15] S. Schwager, S. Renner, T. Hemmerle, S. Karaman, S.T. Proulx, R. Fetz, A.M. Golding-Ochsenbein, P. Probst, C. Halin, D. Neri, M. Detmar, Antibody-mediated delivery of VEGF-C potently reduces chronic skin inflammation, JCI Insight 3 (2018), doi: 10.1172/jci.insight.124850.
[16] R. Doliana, M. Mongiat, F. Bucciotti, E. Giacomello, R. Deutzmann, D. Volpin, G.M. Bressan, A. Colombatti, EMILIN, a component of the elastic fiber and a new member of the C1q/tumor necrosis factor superfamily of proteins, J.Biol. Chem. 274 (1999) 16773–16781.
[17] A. Colombatti, R. Doliana, S. Bot, A. Canton, M. Mongiat, G. Mungiguerra, S. Paron-Cilli, P. Spessotto, The EMILIN protein family, Matrix Biol. 19 (2000) 289–301.
[18] L. Zacchigna, C. Vecchione, A. Notte, M. Cordenonsi, S. Dupont, S. Maretto, G. Cifelli, A. Ferrari, A. Maffei, C. Fabbro, P. Braghetta, G. Marino, G. Selvetella, A. Aretini, C. Colonnese, U. Bettarini, G. Russo, S. Soligo, M. Adorno, P. Bonaldo, D. Volpin, S. Piccolo, G. Lembo, G.M. Bressan, Emilin1 links TGF-beta maturation to blood pressure homeostasis, Cell 124 (2006) 929–942, doi: 10.1016/j.cell.2005.12.035.
[19] G.M. Bressan, D. Daga-Gordini, A. Colombatti, I. Castellani, V. Marigo, D. Volpin, Emilin, a component of elastic fibers preferentially located at the elastin-microfibrils interface, J. Cell Biol. 121 (1993) 201–212.
[20] C. Danussi, A. Petrucco, B. Wassermann, E. Pivetta, T.M. Modica, L. Del Bel Belluz, A. Colombatti, P. Spessotto, EMILIN1-α4/α9 integrin interaction inhibits dermal fibroblast and keratinocyte proliferation, J.Cell Biol. 195 (2011) 131–145, doi: 10.1083/jcb.201008013.
[21] M. Mongiat, G. Mungiguerra, S. Bot, M.T. Mucignat, E. Giacomello, R. Doliana, A. Colombatti, Self-assembly and supramolecular organization of EMILIN, J.Biol.Chem. 275 (2000) 25471–25480, doi: 10.1074/jbc.M001426200.
[22] P. Spessotto, M. Cervi, M.T. Mucignat, G. Mungiguerra, I. Sartoretto, R. Doliana, A. Colombatti, beta 1 Integrin-dependent cell adhesion to EMILIN-1 is mediated by the gC1q domain, J.Biol.Chem. 278 (2003) 6160–6167, doi: 10.1074/jbc.M208322200.
[23] C. Danussi, L. Del Bel Belluz, E. Pivetta, T.M. Modica, A. Muro, B. Wassermann, R. Doliana, P. Sabatelli, A. Colombatti, P. Spessotto, EMILIN1/alpha9beta1 integrin interaction is crucial in lymphatic valve formation and maintenance, Mol.Cell Biol. 33 (2013) 4381–4394, doi: 10.1128/MCB.00872-13.
[24] R. Doliana, S. Bot, P. Bonaldo, A. Colombatti, EMI, a novel cysteine-rich domain of EMILINs and other extracellular proteins, interacts with the gC1q domains and participates in multimerization, FEBS Lett. 484 (2000) 164–168.
[25] C. Danussi, A. Petrucco, B. Wassermann, T.M. Modica, E. Pivetta, L. Del Bel Belluz, A. Colombatti, P. Spessotto, An EMILIN1-negative microenvironment promotes tumor cell proliferation and lymph node invasion, Cancer Prev.Res. (Phila) 5 (2012) 1131–1143, doi: 10.1158/1940-6207.CAPR-12-0076-T.
[26] C. Danussi, P. Spessotto, A. Petrucco, B. Wassermann, P. Sabatelli, M. Montesi, R. Doliana, G.M. Bressan, A. Colombatti, Emilin1 deficiency causes structural and functional defects of lymphatic vasculature, Mol.Cell Biol. 28 (2008) 4026–4039, doi: 10.1128/MCB.02062-07.
[27] E. Pivetta, B. Wassermann, L. Del Bel Belluz, C. Danussi, T.M. Modica, O. Maiorani, G. Bosisio, F. Boccardo, V. Canzonieri, A. Colombatti, P. Spessotto, Local inhibition of elastase reduces EMILIN1 cleavage reactivating lymphatic vessel function in a mouse lymphoedema model, Clin. Sci. (Lond.) 130 (2016) 1221–1236, doi: 10.1042/CS20160064.
[28] A. Capuano, F. Fogolari, F. Bucciotti, P. Spessotto, P.A. Nicolosi, M.T. Mucignat, M. Cervi, G. Esposito, A. Colombatti, R. Doliana, The α4β1/EMILIN1 interaction discloses a novel and unique integrin-ligand type of engagement, Matrix Biol. 66 (2018) 50–66, doi: 10.1016/j.matbio.2017.10.001.
[29] A. Capuano, E. Pivetta, F. Baldissera, G. Bosisio, B. Wassermann, F. Bucciotti, A. Colombatti, P. Sabatelli, R. Doliana, P. Spessotto, Integrin binding site within the gC1q domain orchestrates EMILIN-1-induced lymphangiogenesis, Matrix Biol. 81 (2019) 34–49, doi: 10.1016/j.matbio.2018.10.006.
[30] R.P. Nair, K.C. Duffin, C. Helms, J. Ding, P.E. Stuart, D. Goldgar, J.E. Gudjonsson, Y. Li, T. Tejasvi, B.J. Feng, A. Ruether, S. Schreiber, M. Weichenthal, D. Gladman, P. Rahman, S.J. Schrodi, S. Prahalad, S.L. Guthery, J. Fischer, W. Liao, P.Y. Kwok, A. Menter, G.M. Lathrop, C.A. Wise, A.B. Begovich, J.J. Voorhees, J.T. Elder,

G.G. Krueger, A.M. Bowcock, G.R. Abecasis, Collaborative association study of psoriasis, genome-wide scan reveals association of psoriasis with IL-23 and NF-kappaB pathways, Nat. Genet. 41 (2009) 199–204, doi: 10.1038/ng.311.

[31] E. Pivetta, C. Danussi, B. Wassermann, T.M. Modica, L. Del Bel Belluz, V. Canzonieri, A. Colombatti, P. Spessotto, Neutrophil elastase-dependent cleavage compromises the tumor suppressor role of EMILIN1, Matrix Biol. 34 (2014) 22–32, doi: 10.1016/j.matbio.2014.01.018.

[32] O. Maiorani, E. Pivetta, A. Capuano, T.M. Modica, B. Wassermann, F. Bucciotti, A. Colombatti, R. Doliana, P. Spessotto, Neutrophil elastase cleavage of the gC1q domain impairs the EMILIN1-alpha4beta1 integrin interaction, cell adhesion and anti-proliferative activity, Sci. Rep. 7 (2017) 39974, doi: 10.1038/srep39974.

[33] R. Zheng, W.M. Longmate, L. DeFreest, S. Varney, L. Wu, C.M. DiPersio, L. Van De Water, Keratinocyte integrin $\alpha 3\beta 1$ promotes secretion of IL-1α to effect paracrine regulation of fibroblast gene expression and differentiation, J. Invest. Dermatol. 139 (2019) 2029-2038.e3, doi: 10.1016/j.jid.2019.02.025.

[34] H.H. Hu, D.Q. Chen, Y.N. Wang, Y.L. Feng, G. Cao, N.D. Vaziri, Y.Y. Zhao, New insights into TGF-β/Smad signaling in tissue fibrosis, Chem. Biol. Interact. 292 (2018) 76–83, doi: 10.1016/j.cbi.2018.07.008.

[35] K.W. Finnson, Y. Almadani, A. Philip, Non-canonical (non-SMAD2/3) TGF-β signaling in fibrosis: mechanisms and targets, Semin. Cell Dev. Biol. 101 (2020) 115–122, doi: 10.1016/j.semcdb.2019.11.013.

[36] C.A. Steiner, E.S. Rodansky, L.A. Johnson, J.A. Berinstein, K.C. Cushing, S. Huang, J.R. Spence, P.D.R. Higgins, AXL is a potential target for the treatment of intestinal fibrosis, Inflamm. Bowel Dis. 27 (2021) 303–316, doi: 10.1093/ibd/izaa169.

[37] L. Landolt, J. Furriol, J. Babickova, L. Ahmed, Ø. Eikrem, T. Skogstrand, A. Scherer, S. Suliman, S. Leh, J.B. Lorens, G. Gausdal, H.P. Marti, T. Osman, AXL targeting reduces fibrosis development in experimental unilateral ureteral obstruction, Physiol. Rep. 7 (2019) e14091, doi: 10.14814/phy2.14091.

[38] P. Govindaraju, L. Todd, S. Shetye, J. Monslow, E. Puré, CD44-dependent inflammation, fibrogenesis, and collagenolysis regulates extracellular matrix remodeling and tensile strength during cutaneous wound healing, Matrix Biol. 75−76 (2019) 314–330, doi: 10.1016/j.matbio.2018.06.004.

[39] M. Mack, Inflammation and fibrosis, Matrix Biol. 68−69 (2018) 106–121, doi: 10.1016/j.matbio.2017.11.010.

[40] H.M. McGettrick, L.M. Butler, C.D. Buckley, G.E. Rainger, G.B. Nash, Tissue stroma as a regulator of leukocyte recruitment in inflammation, J. Leukoc. Biol. 91 (2012) 385–400, doi: 10.1189/jlb.0911458.

[41] J. Arasa, M.C. Terencio, R.M. Andrés, A. Marín-Castejón, F. Valcuende-Cavero, M. Payá, M.C. Montesinos, Defective induction of COX-2 expression by psoriatic fibroblasts promotes pro-inflammatory activation of macrophages, Front. Immunol. 10 (2019) 536, doi: 10.3389/fimmu.2019.00536.

[42] I. Malyshev, Y. Malyshev, Current concept and update of the macrophage plasticity concept: intracellular mechanisms of reprogramming and m3 macrophage “switch” phenotype, Biomed Res. Int. 2015 (2015) 341308, doi: 10.1155/2015/341308.

[43] G. Favero, A. Paini, C. De Ciuceis, L.F. Rodella, E. Moretti, E. Porteri, C. Rossini, S. Ministrini, L. Solaini, C. Stefano, M.A. Coschignano, V. Brami, A. Petelca, M. Nardin, I. Valli, G.A.M. Tiberio, F. Bonomini, C. Agabiti Rosei, N. Portolani, D. Rizzoni, R. Rezzani, Changes in extracellular matrix in subcutaneous small resistance arteries of patients with essential hypertension, Blood Press. 27 (2018) 231–239, doi: 10.1080/08037051.2018.1448256.

[44] P.M. Angel, D.A. Narmoneva, M.K. Sewell-Loftin, C. Munjal, L. Dupuis, B.J. Landis, A. Jegga, C.B. Kern, W.D. Merryman, H.S. Baldwin, G.M. Bressan, R.B. Hinton, Proteomic alterations associated with biomechanical dysfunction are early processes in the Emilin1 deficient mouse model of aortic valve disease, Ann. Biomed. Eng. 45 (2017) 2548–2562, doi: 10.1007/s10439-017-1899-0.

[45] C. Munjal, A.M. Opoka, H. Osinska, J.F. James, G.M. Bressan, R.B. Hinton, TGF-beta mediates early angiogenesis and latent fibrosis in an Emilin1-deficient mouse model of aortic valve disease, Dis. Model. Mech 7 (2014) 987–996, doi: 10.1242/dmm.015255.

[46] C. Munjal, A.G. Jegga, A.M. Opoka, I. Stoilov, R.A. Norris, C.J. Thomas, J.M. Smith, R.P. Mecham, G.M. Bressan, R.B. Hinton, Inhibition of MAPK-Erk pathway *in vivo* attenuates aortic valve disease processes in Emilin1-deficient mouse model, Physiol. Rep. 5 (2017) e13152, doi: 10.14814/phy2.13152.

[47] S. Chen, Q. Wu, Y. Wang, J. Xu, Y. Wang, X. Luo, miR-491-5p inhibits Emilin 1 to promote fibroblasts proliferation and fibrosis in gluteal muscle contracture via TGF-β1/Smad2 pathway, Physiol. Res. 71 (2022) 285–295 PMID: 35275699, doi: 10.33549/physiolres.934804.

[48] S.H. Lin, H.Y. Chuang, J.C. Ho, C.H. Lee, C.C. Hsiao, Treatment with TNF-α inhibitor rectifies M_1 macrophage polarization from blood $CD_{14}+$ monocytes in patients with psoriasis independent of $STAT_1$ and IRF-$_1$ activation, J. Dermatol. Sci. 91 (2018) 276–284, doi: 10.1016/j.jdermsci.2018.05.009.

[49] K. Furue, T. Ito, G. Tsuji, T. Kadono, M. Furue, Psoriasis and the TNF/IL_{23}/IL_{17} axis, G. Ital. Dermatol. Venereol. 154 (2019) 418–424, doi: 10.23736/S0392-0488.18.06202-8.

[50] U. Lichti, J. Anders, S.H. Yuspa, Isolation and short-term culture of primary keratinocytes, hair follicle populations and dermal cells from newborn mice and keratinocytes from adult mice for *in vitro* analysis and for grafting to immunodeficient mice, Nat. Protoc 3 (2008) 799–810, doi: 10.1038/nprot.2008.50.

[51] P. Spessotto, E. Giacomello, R. Perri, Improving fluorescence-based assays for the *in vitro* analysis of cell adhesion and migration, Mol. Biotechnol. 20 (2002) 285–304.